Sensitivity of gold nanoparticles Second Harmonic scattering to surrounding medium change

Krzysztof Nadolski, Christian Jonin, Estelle Salmon, Zacharie Behel, Katarzyna Matczyszyn, Pierre-François Brevet

Sensitivity of Gold Nanoparticles Second Harmonic Scattering to Surrounding Medium Change

Krzysztof Nadolski,[1,2] Christian Jonin,[1] Estelle Salmon,[1] Zacharie Behel,[1]

Katarzyna Matczyszyn,[2] Pierre-François Brevet[1*]*

[1]Institut Lumière Matière, Université Claude Bernard Lyon 1, CNRS UMR 5306, Villeurbanne, France.

[2]Institute of Advanced Materials, Wroclaw University of Science and Technology, Wroclaw, Poland.

KEYWORDS: gold nanoparticles, nonlinear optics, second harmonic scattering, refractive index, sensing

* Corresponding authors: Prof. Katarzyna Matczyszyn, katarzyna.matczyszyn@pwr.edu.pl

Prof. Pierre-François Brevet, pfbrevet@univ-lyon1.fr

ABSTRACT

Gold nanoparticles are widely used in sensing, notably in colorimetry-based methods, where a color change is associated to the Surface Plasmon Resonance peak shift due to a binding event or an environment modification in the vicinity of the nanoparticles. In this work, we explore the sensitivity of the Second Harmonic response from gold nanoparticles of two different diameters as this response stems principally from the nanoparticle surface at small sizes as opposed to the whole volume of the nanoparticle at larger sizes. The origin of this response is therefore different from that involved in the colorimetric response, the latter being of volume origin. Upon addition of Glycerol to an aqueous solution of nanoparticles, Surface Plasmon Resonance peak shifts are first observed but they cannot fully explain the Second Harmonic intensity changes recorded. Hence, in order to gain further insights into the origin of the changes observed in the experimental data, polarization-resolved Second Harmonic measurements are performed. A mechanism where first a modification of the first hyperpolarizability of the nanoparticles due to the presence of glycerol occurs followed by nanoparticle aggregation is then proposed. The potential alternative use of this nonlinear optical method of Second Harmonic scattering for sensing purposes is then discussed in light of a figure of merit proposed to describe the sensing sensitivity observed.

1. INTRODUCTION

Sensitive and quantitative detection of chemical or biological compounds is currently of utmost importance in many applications, from biomedical or forensic sciences to environmental studies. Among the diverse methods available to date, gold nanoparticles (AuNPs) based sensors are attracting a lot of attention due in particular to the AuNPs properties like high surface-to-volume ratio or tunable optical properties.[1-3] These properties can be easily tailored through changes of the AuNPs size or shape in view of the sensor applications targeted.[4, 5] Among the different methods involving AuNPs, optical ones have retained a lot of attention as they enable simple experimental designs. AuNPs exhibit Localized Surface Plasmon Resonances (LSPR) resulting from the interaction of the incident light with the conduction band electrons.[6] Hence, colorimetric methods based on linear optical extinction have been proposed with success.[7-10] Such LSPR based sensing methods rely on the spectral properties of the LSPR and the ability to modify them through the sensing process, in particular through a change of the surrounding medium refractive index.[11]

Within this context of sensing, nonlinear optics based sensors are promising owing to the dependence of the sensor response to higher powers of the incident light intensity as opposed to the above described linear optical methods like extinction and scattering, where the response is linear with the incident light intensity.[12] For instance, Third Harmonic Generation (THG), namely the conversion of three photons into a single photon at the sum energy, has yielded in simple plasmonic antennas limits of detection of the order of $\Delta n \approx 10^{-3}$ where Δn is the surrounding medium refractive index change.[13, 14] Also, the nonlinear optical response stems from the surface as opposed to the volume for even order nonlinear processes. A greater sensitivity

is thus expected along with better limits of detection in the latter case. Therefore, Second Harmonic Generation (SHG), the quadratic nonlinear optical phenomenon whereby two incident photons are annihilated and a single photon at the sum energy emitted is attracting interest due to its inherent surface origin when performed with gold nanoparticles (AuNPs). [14, 15] In its most simple design, the SHG signal is scattered from an AuNPs aqueous suspension, a phenomenon called Hyper Rayleigh Scattering (HRS). It has been widely described for Au spheres, rods or prisms[16-18] for NPs sizes ranging from 150 nm down to 2.5 nm and Au nanoclusters where the LSPR vanishes due to the loss of the metallic character.[19] However, it is though of utmost importance to assess the exact origin of the HRS response because competing processes may dominate instead of the expected surface response. This is the case of aggregation that can occur when the stability of the nanoparticles suspension is broken. Similarly to colorimetric methods, HRS sensing can still be based on the LSPR spectral shift. In this case, the gain lies in the power dependence of the observed intensity with the LSPR spectral shift. The HRS intensity remains nevertheless weak. A possibility is thus to define a figure-of-merit (FoM) less prone to intensity fluctuations.[3, 20] The latter can be defined as the ratio between the sensitivity, namely the LSPR shift in nanometers divided by the refractive index change and the full width at half maximum (FWHM) as proposed by Sherry et al..[21] It has been shown that sensing based on multipolar LSPR resonant SHG can already enhance the sensitivity but that the above defined FoM allows to identify an optimal size for the spherical nanoparticles depending on the material, gold or silver for instance.[22]

In the present work, the potential for sensing of AuNPs in the context of HRS is investigated further using a water-glycerol mixture as the surrounding medium. The standard right-angle HRS configuration is used and the study is devoted to the intensity and polarization analysis of the

response. The first part of our study focuses on the mechanisms involved as glycerol is introduced into an aqueous suspension of gold nanoparticles and the origin of the response is assessed. In particular, the role of nanoparticle surface changes and aggregation are discussed as well as the role of the LSPR spectra shift in the HRS intensity and polarization changes. In the second part, the sensitivity to the refractive index change is discussed in view of sensing purposes. Two gold nanoparticle sizes were selected, namely 40 nm and 100 nm diameter nanoparticles. The smaller 40 nm nanoparticles are expected to possess a nonlinearity of surface origin whereas the larger 100 nm ones are expected to have a dominant volume origin for their nonlinearity [14, 18].

2. EXPERIMENTAL

Citrate stabilized AuNPs with a mean diameter of 40 and 100 nm were purchased (BBI Solutions) and used as received. To change the refractive index, water-glycerol mixtures were prepared from ultra-pure water (MilliQ Millipore, resistivity 18 MΩ) and glycerol (Archem Sp. z o. o.). The solution refractive index was measured on an Abbe refractometer for the sodium D-line at $\lambda = 589$ nm. The UV-Visible extinction spectra were measured on a standard spectrophotometer (Jasco, model V670).

The Hyper Rayleigh Scattering setup has been described elsewhere.[14] Briefly, the laser beam of a Ti:Sapphire femtosecond laser operating at the wavelength of 820 nm with pulse length of about 140 fs and repetition rate of 80 MHz was gently focused with a X16 objective into the fused silica cell. A low bandpass filter was placed prior to the objective to remove any unwanted SHG light generated prior to the cell. The average input power was kept at about 300 mW. The SHG intensity

was collected at right angle with a CCD camera placed after a spectrometer. Polarization analysis was performed with a half-wave plate and a cube polarizer to select the polarization of the scattered harmonic light, either vertically or horizontally linearly polarized, while preserving the polarization of the detected light and a second half-wave plate was placed on the fundamental beam path to select the linear input polarization angle. Long bandpass filters were placed right after the cell to remove any unwanted spurious fundamental scattered light. Absorbances were always kept low enough in order to avoid any spurious higher order nonlinear effects.

3. RESULTS AND DISCUSSION

Spherical AuNPs with two different sizes, namely 40 and 100 nm diameter, were studied to investigate the role of the NP size. Here, we have focused on spherical nanoparticles in order to perform through the two different sizes a comparison of the surface to volume origin of the nonlinearity. Other shapes are possible but would further complexify the present analysis. Different amounts of glycerol were added to the AuNPs aqueous solutions resulting in samples containing from 0 up to 75 volume percent of glycerol. Because the solutions were purchased as aqueous suspensions and to prevent a too large dilution of the nanoparticles, 75 volume percent of glycerol was chosen as the upper limit for the glycerol content. A simple analysis of the optical index as a function of the glycerol content with the Lorentz-Lorenz equation underlined the ideality of the mixed water-glycerol system within the range of glycerol volume content studied, see Figure S1 in Supplementary File.[23] The UV-Visible extinction spectra were collected to observe the red-shift of the LSPR peak along with the extinction increase on the red side of the spectra as the glycerol content increases, resulting in a change of the solvent refractive index, see Figures 1(a),(b). As expected, the position of the LSPR peak red-shifted linearly with increasing

glycerol content as the refractive index of the solution increased, see Figures S2(a)-(d). Also, for the 40 nm diameter gold nanoparticles, aggregation is observed through the increase of the extinction cross-section at 800 nm, a feature not so prominent for 100 nm diameter gold nanoparticles due to the broadening of the LSPR for this nanoparticle size hiding this phenomenon. No change in cross-section is observed at the harmonic wavelength, neither 395 nm nor 410 nm, for 40 nm diameter gold nanoparticles whereas a weak change occurs for 100 nm diameter ones, a small decrease around 400 nm and a small increase at the fundamental wavelength of 800 nm.

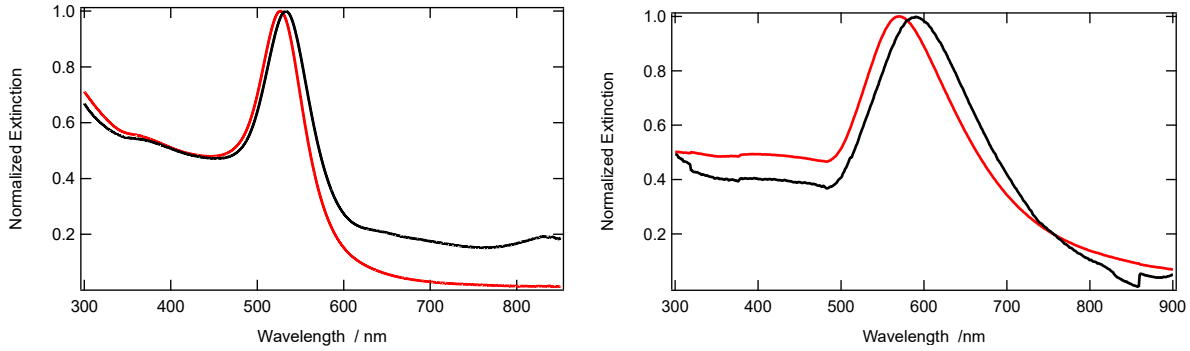

(a) (b)

Figure 1: Normalized UV-Visible extinction spectra for (a) 40 nm and (b) 100 nm AuNPs nanosphere diameter for two different glycerol percent fraction, (red) pure water solution, (black) 2/3 glycerol volume fraction.

The HRS intensity from the different AuNPs sample solutions was then collected for the 790 nm and 820 nm fundamental wavelengths, resulting in an HRS wavelength at 395 nm and 410 nm respectively, see Figures 2(a)-(b) for the two nanoparticle diameters of 40 nm and 100 nm. The

intensity was renormalized for the nanoparticle content as glycerol addition into the aqueous AuNPs solutions leads to dilution. This renormalization procedure did not signficantly affect the observed features in Figures 2(a)-(b) but was deemed necessary for further quantitative analysis. No significant differences in intensity behaviour were observed between the two 790 nm and 820 nm fundamental wavelengths. Results at 820 nm are therefore exhibited below, see Supplementary Information file Figures S3(a)-(b), for data collected at 790 nm fundamental wavelength.

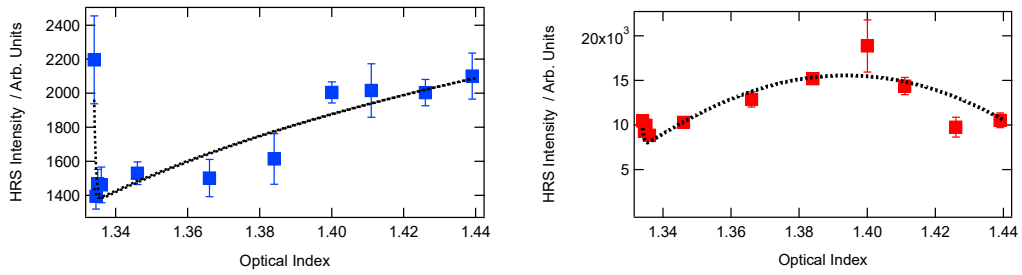

(a) **(b)**

Figure 2: HRS intensity measured at 820 nm fundamental wavelength for (a) 40 nm and (b) 100 nm spherical AuNPs dispersed in water-glycerol mixtures with different glycerol additions. HRS intensities are renormalized for nanoparticles concentration. (Black dashed): adjusted curve using the model described below.

From the observed HRS intensity, three main features are observed. First, a sharp decrease of the HRS intensity is observed at extremely small glycerol content followed by a recovery as the glycerol content increases. These two features are observed for both the 40 nm and 100 nm diameter gold nanoparticles whereas a third feature is observed for 100 nm diameter nanoparticles,

namely a decrease of the HRS intensity when the glycerol volume fraction gets larger than that of water. To rationalize these features into physical mechanisms, the role of the LSPR peak shift must be discussed beforehand. The SHG response from small metallic nanoparticles like gold or silver nanoparticles can be described within the Mie theory. In this context, the response essentially stems from the nanoparticle surface but local fields and their associated Mie resonances must be taken into account. Electric dipole E1 and quadrupole E2 resonances associated to the corresponding modes must be considered.[22-25] The pure electric dipole and quadrupole responses, respectively I_D and I_Q, are of the following form [25]:

$$I_D = \kappa|\beta_D|^2 \left[\frac{1}{\varepsilon_{Au}(410nm)+2\varepsilon_s}\right]^2 \left[\frac{1}{\varepsilon_{Au}(820nm)+2\varepsilon_s}\right]^4 \quad (1a)$$

$$I_Q = \kappa|\beta_Q|^2 \left[\frac{1}{2\varepsilon_{Au}(410nm)+3\varepsilon_s}\right]^2 \left[\frac{1}{\varepsilon_{Au}(820nm)+2\varepsilon_s}\right]^4 \quad (1b)$$

where β_D and β_Q are two parameters scaling the nanoparticle surface response and ε_{Au} and ε_s are the dielectric constants of gold [26] and the water-glycerol solvent. The constant κ accounts for all other parameters except the local field factors, strongly refractive index dependent, that are made explicit. In principle, β_D and β_Q are identical, both stemming from the AuNPs surface response. Note that in Eq.(1b), only the quadrupole response at the harmonic frequency is considered as the latter is susceptible to resonance enhancement due to the proximity of the harmonic wavelength with the electric quadrupole resonance wavelength. Figure 3 shows the evolution of the dipolar and quadrupolar responses I_D and I_Q with respect to the refractive index

of the surrounding medium, plotted according to Eqs.1(a)-(b). It appears that both I_D and I_Q intensities are slowly decreasing over the whole range of the glycerol-water mixture refractive index whereas the HRS experiments exhibit the reverse, see Figures 2, and at least partially for the 100 nm diameter AuNPs. Thus, it is concluded that the change of the refractive index of the surrounding medium is not responsible for the observed experimental behaviour, except possibly for the 100 nm diameter AuNPs at refractive indices larger than 1.40. It is also noted that at very low glycerol contents, the drop in HRS intensity is abrupt as opposed to the general behaviour observed over the whole range of the refractive index change. The latter drop is therefore not related to the refractive index change either.

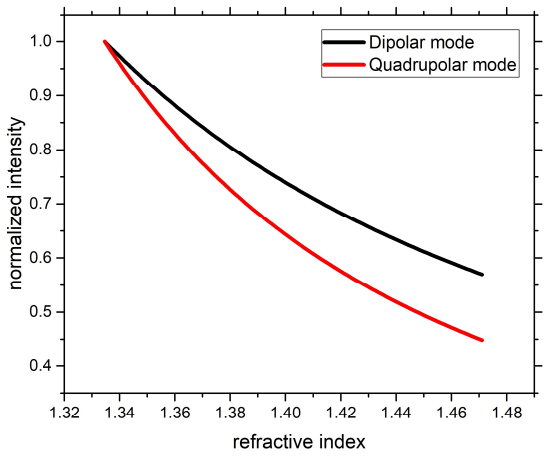

Figure 3: Normalized theoretical (black) dipolar and (red) quadrupolar response to the SHG intensity as a function of the refractive index change of the mixed water-glycerol solvent.

Hence, to explain the behaviour observed experimentally, the following mechanisms are introduced, in line with previous works.[27] First, at very low glycerol content, it is expected that the surface hyperpolarizability of the nanoparticles is modified according to the following law :

$$\beta_m = \beta_{0m} + \triangle\beta e^{-\alpha[n-n_W]} \quad (2)$$

where the second term is the change of the surface hyperpolarizability with the glycerol content through the solution optical index n, whereas that of neat water is n_W, and β_{0m} and $\beta_{0m} + \Delta\beta$ are the first hyperpolarizability of a gold nanoparticle in glycerol and water respectively. An exponential decrease scaling with the parameter α is introduced in an ad-hoc fashion in order to distinguish the local changes at the nanoparticle surface at very low glycerol content as compared to the solvent optical index changes effectively accounted for with the above Eqs.1(a)-(b) and Figure 3. The local glycerol interaction with the nanoparticle surface saturates at high enough glycerol content. Second, and in agreement with the increase of extinction for the 40 nm diameter nanoparticles around 800 nm, see Figure 1(a), slow aggregation is observed. The latter phenomenon is described with an equilibrium constant between nanoparticle monomers and dimers with an equilibrium constant, the scaling of which is linearized with respect to the solution optical index due to the rather weak aggregation strength. As a result, the HRS intensity is given by :

$$I_{HRS} = G[N_m\langle\beta_m^2\rangle + N_d\langle\beta_d^2\rangle] \quad (3)$$

In Eq.(3), N_m and N_d are the monomer and dimer concentrations and $\langle\beta_m^2\rangle$ and $\langle\beta_d^2\rangle$ the square of their first hyperpolarizability averaged over all orientations and G is a general parameter incorporating all other physical constants. We underline here the fact that these nanoparticles cannot be considered as perfect sphere and therefore the orientational averaging is required. Furthermore, the $\langle\beta_d^2\rangle$ dimer hyperpolarizability is assumed constant because the local interactions with glycerol only occur at very low glycerol content when aggregation is negligible. Finally, the total number of nanoparticles is taken constant. With this rather simple model, the experimental data are well described, see adjusted curves in Figures 2(a)-(b), except at high glycerol content for the 100 nm diameter nanoparticles. In this range of glycerol content, it is expected that aggregation further proceeds towards larger aggregates with the net result of the HRS intensity decrease. This feature suggests that larger aggregates have a much smaller hyperpolarizability as compared to smaller ones, once normalized per nanoparticle in the aggregate. Saturation of this hyperpolarizability has already been observed in pyridine induced aggregation.[28] Note that considering the monomer-dimer and larger aggregates equilibria only greatly simplifies a problem where multiple nanoparticle aggregates equilibria are certainly involved.

To get a deeper insight into the HRS response of the AuNPs with respect to the surrounding medium change, polarization-resolved measurements were also conducted. To perform these studies, an analyzer was placed prior to the detection system. All polar plots are included in the Supporting Information file, see Figures S4 and S5 for the 40 nm and 100 nm diameter

respectively. A full analysis was performed in order to extract a quantitative analysis from the data. The graphs were adjusted with the following expression for the HRS intensity I^X :[14, 29]

$$I^X = a^X cos^4\gamma + b^X cos^2\gamma\, sin^2\gamma + c^X sin^4\gamma \quad (4)$$

where X stands for H (horizontal, i.e. parallel to the plane of scattering) or V (vertical, i.e. perpendicular to the plane of scattering) output polarization, a^X, b^X and c^X are three intensity parameters and γ is the polarization angle of the fundamental wavelength field. All intensity parameters are of the form of Eq.(3) where distinct hyperpolarizability tensor elements have to be considered depending on the output polarization and the fundamental input polarization angle γ. Analysis of the polarization plots allows to introduce specific parameters, using the intensity parameters obtained with the adjustment procedure of the two perpendicular polarization experimental data with Eq.(4). The depolarization ratio, D^V, is defined as[14]:

$$D^V = c^V/a^V \quad (5)$$

whereas the retardation parameters $\zeta^V$and ζ^H are introduced as follows[18, 29, 30]:

$$\zeta^V = (b^V - a^V - c^V)/b^V \quad (6a)$$

$$\zeta^H = (a^H - c^H)/(a^H + c^H) \quad (6b)$$

The depolarization ratio provides an insight into the nature of the HRS response of the NPs as it weights the dipolar and octupolar contributions to the HRS response within the context of the irreducible representation of the first hyperpolarizability tensor.[31] On the opposite, the two ζ^V

and ζ^H parameters provide a measure of the extent of retardation in the response. Retardation describes the evolution of the spatial phase over the nanoparticle size. Hence, size will lead to values of these parameters deviating from zero whereas deviation from a centrosymmetric shape decreases these parameters as it enhances the surface local nonlinearity. The dependence of these three parameters with the refractive index is depicted in Figures 4(a)-(f). Uncertainties were calculated by the exact differential method using uncertainties from the adjustment of the experimental data with Eq.(4). Polar graphs and their fits to Eq.(4) are provided in the Supporting Information file, Figures S4(a)-(j), S5(a)-(v).

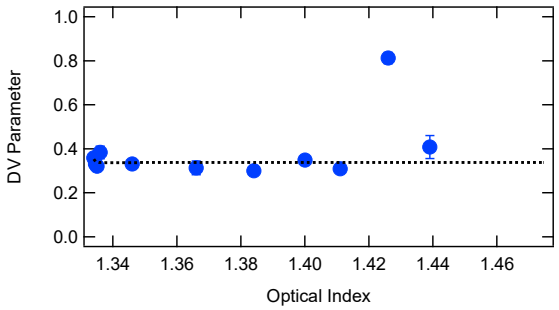

(a)

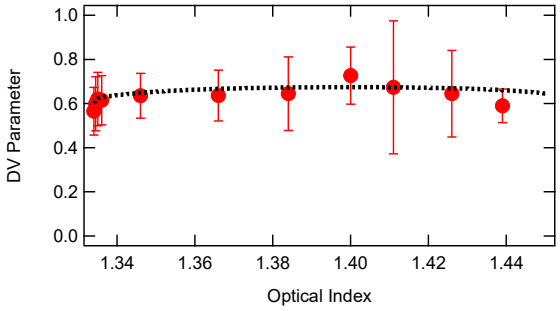

(b)

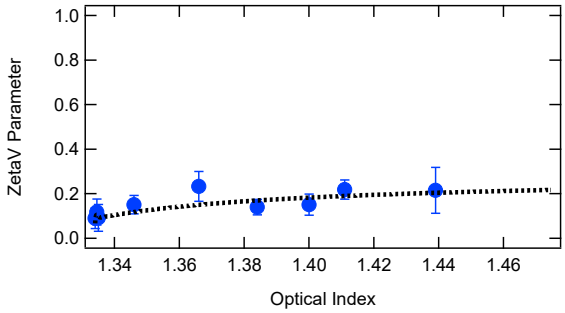

(c)

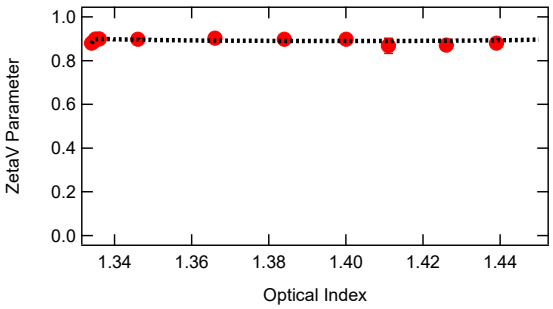

(d)

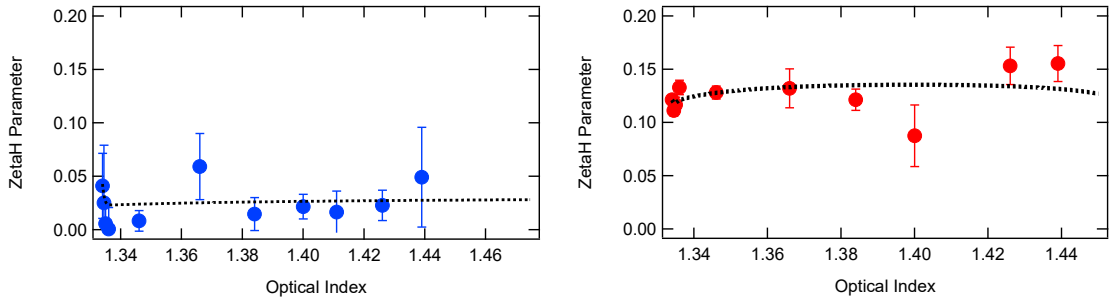

(e) (f)

Figure 4: (a-b) Depolarization ratio and (c-d) retardation parameters for Vertically and (e-f) Horizontally polarized HRS intensity with respect to the surrounding medium refractive index for (blue; a, c, e) 40 nm and (red; b, d, f) 100 nm diameter AuNPs.

For the 40 nm diameter AuNPs, the depolarization ratio D^V remains in the range 0.30-0.40 indicating a rather similar contribution from the dipolar and octupolar irreducible tensor contributions.[27] These values are rather similar to what has been observed for AuNPs with similar sizes. Adjustment of the experimental depolarization ratio D^V is then achieved with the above model for the HRS intensity as a function of the glycerol-water mixture optical index, with account of the selection of the hyperpolarizability tensor elements of the monomers and aggregates with the output polarization selection. On the opposite, the 100 nm diameter AuNPs exhibit an almost purely octupolar response with a D^V coefficient close to 2/3. Retardation parameters ζ^V and ζ^H do not take large values for 40 nm diameter AuNPs as expected, only for the 100 nm diameter ones do they take large values, also in line with previous works.[28] As a result, marked changes only appear at small glycerol additions on the HRS intensity and are more visible for the 40 nm diameter AuNPs. For larger glycerol additions, changes in the parameters are rather smooth and weak. Similar behaviour was observed for 790 nm excitation wavelength, see Supplementary

Information file, Figures S6(a)-(b). It appears therefore that glycerol at very low content is sufficient to modify the HRS response at the surface of the AuNPs. This effect is more prominent for the smallest nanoparticles and is clearly seen on the HRS intensity plots as well as the characteristic parameters of the response. For the larger 100 nm diameter AuNPs, larger retardation contribution occurs, as seen from the larger retardation parameters. Being of higher order, this contribution scales with the size of the nanoparticles, i.e. their volume, and the surface effect is lost. The nonlinear optical surface response is therefore modified in strength and nature with the incorporation of small amounts of glycerol. The decrease of HRS intensity with almost constant depolarization coefficient indicates a change of the surface nonlinearity with minimal changes in symmetry as seen from the dipolar to octupolar contributions ratio in the context of the irreducible tensorial representation of the hyperpolarizability. This feature in particular suggests that the AuNPs surface probes localized changes. Homogeneity of the refractive index is however recovered at much larger glycerol contents.[31] The present results therefore indicate that the LSPR peak shift with the refractive index in HRS measurements from AuNPs do not play any major role in this study. Rather, the HRS response at small glycerol addition is driven by the surface contribution, especially for the smallest AuNPs. The sensitivity to the localized surface changes indicates that sensing using AuNPs in HRS measurements should be attractive especially at low refractive index changes and small AuNPs sizes. At larger glycerol content, the localized surface changes saturate and aggregation takes place with smooth increase of the HRS intensity. However, as suggested by the extinction spectra, see Figure 1, aggregation is rather weak and therefore the retardation parameters ζ^V and ζ^H are weakly affected because aggregates remain small for 40 nm diameter nanoparticles. For 100 nm diameter nanoparticles, retardation is already too much developed with values close to 0.9 to observe clear changes.

In this respect, this study indicates that sensing with gold nanoparticles must be performed with the smaller gold nanoparticles where surface sensitivity is achieved as compared to larger 100 nm diameter ones. A FoM can thus be defined as opposed to the LSPR peak shift that may not be as adapted as expected. Rather, a FoM based on the change in the HRS intensity should be better suited. A FoM of the form $(\Delta I/I)/RIU$, free from intensity fluctuations with renormalization, may then be built where *RIU* stands for *Refractive Index Unit.* From Figure 2(a), and using the above model adjusted on the experimental data with a first order expansion of Eq.(2) with the optical index change $n - n_W$, this FoM is given by :

$$FoM = \frac{(\Delta I/I)}{RIU} = 2\alpha\Delta\beta \quad (7)$$

the value of which is about 4000 considering the numerical values obtained from the model adjusted to the data. Such a FoM value suggests a sensitivity of the order of less than 1% in glycerol volume content considering Figure S1 linking the optical index to the volume fraction of glycerol. This analysis therefore provides a quantitative assessment of the sensing ability of smaller gold nanoparticles HRS towards small refractive index changes.

4. CONCLUSIONS

The HRS intensity of AuNPs with a 40 nm and 100 nm mean diameter dispersed in water was studied after addition of different amounts of glycerol. Marked changes are exhibited at the lowest glycerol additions before an intensity recovery, features attributed to initial local surface changes of the nanoparticle first hyperpolarizability followed by a weak aggregation. Polarization-resolved studies are performed to assess the origin and nature of the nonlinear response. For larger glycerol additions, changes are not so pronounced and rather smooth. These features are more prominent for the 40 nm diameter nanoparticles as opposed to the 100 nm diameter ones.

UV-Visible extinction based colorimetric measurements do not allow to attribute the changes at very low glycerol contents, namely below 1 vol. %, to the linear wavelength shift of the SPR peak. For this purpose, the HRS method is more advantageous as it exhibits more pronounced signal changes. This property of the HRS method is due to the origin of the response stemming from the AuNPs surface at for small diameter nanoparticles as opposed to nanoparticles with larger diameter. Combined with the simplicity of the geometrical arrangements for these measurements, HRS scattering from AuNP solutions is a promising method for sensing applications. This work further indicates that rather small diameter nanoparticles must be used to avoid the detrimental contribution from retardation, still keeping large intensities, and to use the normalized HRS intensity change as a figure of merit. Further works involving more refined platforms to perform sensing have also appeared [32]but HRS remains rather simple into its development.

DECLARATION OF COMPETING INTEREST

The authors declare no competing interest connected with this work.

ACKNOWLEDGEMENTS

K.N. and K.M. acknowledge funding from the National Science Centre in Poland within the Harmonia DEC/2016/22/M/ST4/00275 project and funding from the National Science Centre in Poland within the Opus UMO-2019/35/B/ST4/03280 project. All authors acknowledge funding from the PPN/BFT/2019/1/00030/U/0001 PHC POLONIUM project, cofunded by the Polish National Agency For Academic Exchange and Campus France.

References

1. L. Tessaro, A. Aquino, A. P. Azevedo de Carvalho, C. A. Conte-Junior, *A systematic review on gold nanoparticles based-optical biosensors for Influenza virus detection.* Sensors and Actuators Reports, 2021. **3**: p. 100060.
2. E. Priyadarshini, N. Pradhan, *Gold nanoparticles as efficient sensors in colorimetric detection of toxic metal ions: A review.* Sensors and Actuators B: Chemical, 2017. **238**: p. 888-902.
3. G. Liu, M. Lu, X. Huang, T. Li, D. Xu, *Application of Gold-Nanoparticle Colorimetric Sensing to Rapid Food Safety Screening.* Sensors, 2018. **18**(12).
4. K. Saha, S. S. Agasti, C. Kim, X. Li, V. M. Rotello, *Gold Nanoparticles in Chemical and Biological Sensing.* Chemical Reviews, 2012. **112**(5): p. 2739-2779.
5. A. Moores, F. Goettmann, *The plasmon band in noble metal nanoparticles: an introduction to theory and applications.* New Journal of Chemistry, 2006. **30**: p. 1121-1132.
6. E. Petryayeva, U. J. Krull, *Localized surface plasmon resonance: nanostructures, bioassays and biosensing - a review.* Analytica Chimica Acta, 2011. **1**(706): p. 8-24.
7. J. N. Anker, W. P. Hall, O. Lyandres, N. C. Shah, J. Zhao, R. P. Van Duyne, *Biosensing with plasmonic nanosensors.* Nature Materials, 2008. **7**: p. 442-453.
8. C. Xie, F. Xu, X. Huang, C. Dong, J. Ren, *Single Gold Nanoparticles Counter: An Ultrasensitive Detection Platform for One-Step Homogeneous Immunoassays and DNA Hybridization Assays.* Journal of the American Chemical Society, 2009. **131**(35): p. 12763-12770.
9. N. Nath, A. Chilkoti, *A Colorimetric Gold Nanoparticle Sensor To Interrogate Biomolecular Interactions in Real Time on a Surface.* Analytical Chemistry, 2002. **74**(3): p. 504-509.

10. C-C. Chang, C-P. Chen, T-H. Wu, C-H. Yang, C-W. Lin, C-Y. Chen, *Gold Nanoparticle-Based Colorimetric Strategies for Chemical and Biological Sensing Applications.* Nanomaterials, 2019. **9**(6).
11. A. A. Dormeny, P. A. Sohi, M. Kahrizi, *Design and simulation of a refractive index sensor based on SPR and LSPR using gold nanostructures.* Results in Physics, 2020. **16**.
12. L. Bonacina, P-F. Brevet, M. Finazzi, M. Celebrano, *Harmonic generation at the nanoscale.* Journal of Applied Physics, 2020. **127**: p. 230901.
13. M. Mesch, B. Metzger, M. Hentschel, H. Giessen, *Nonlinear Plasmonic Sensing.* Nano Letters, 2016. **16**(5): p. 3155-3159.
14. J. Nappa, G. Revillod, I. Russier-Antoine, E. Benichou, C. Jonin, P.F. Brevet, *Electric dipole origin of the second harmonic generation of small metallic particles.* Physical Review B, 2005. **71**: p. 165407.
15. L. Ghirardini, A-L. Baudrion, M. Monticelli, D. Petti, P. Biagioni, L. Duo, G. Pellegrini, P-M. Adam, M. Finazzi, M. Celebrano, *Plasmon-Enhanced Second Harmonic Scattering.* The Journal of Physical Chemistry C, 2018. **122**(21): p. 11475-11481.
16. Y. El Harfouch, E. Benichou, F. Bertorelle, I. Russier-Antoine, C. Jonin, N. Lascoux, P-F. Brevet, *Hyper-Rayleigh Scattering from Gold Nanorods.* The Journal of Physical Chemistry C, 2014. **118**: p. 609-616.
17. E. C. Hao, G. C. Schatz, R. C. Johnson, J. T. Hupp, *Hyper-Rayleigh scattering from silver nanoparticles.* The Journal of Chemical Physics, 2002. **117**: p. 5963.
18. K. Nadolski, E. Benichou, N. Tarnowicz-Staniak, A. Żak, C. Jonin. K. Matczyszyn, P-F. Brevet, *Adverse Role of Shape and Size in Second-Harmonic Scattering from Gold Nanoprisms.* The Journal of Physical Chemistry C, 2020. **124**: p. 14797-14803.
19. R. Jin, C. Zeng, M. Zhou, Y. Chen, *Atomically Precise Colloidal Metal Nanoclusters and Nanoparticles: Fundamentals and Opportunities.* Chemical Reviews, 2016. **116**(18): p. 10346-10413.
20. S. Unser, I. Bruzas, J. he, L. Sagle, *Localized Surface Plasmon Resonance Biosensing: Current Challenges and Approaches.* Sensors, 2015. **15**: p. 15684-15716.
21. L. J. Sherry, S-H. Chang, G. C. Schatz, R. P. Van Duyne, B. J. Wiley, Y. Xia, *Localized Surface Plasmonc Resonance Spectroscopy of Single Silver Nanocubes.* Nano Letters, 2005. **5**(10): p. 2034-2038.
22. J. Butet, I. Russier-Antoine, C. Jonin, N. Lascoux, E. Benichou, P-F. Brevet, *Sensing with Multipolar Second Harmonic Generation from Spherical Metallic Nanoparticles.* Nano Letters, 2012. **12**(3): p. 1697-1701.
23. J. I. Dadap, J. Shan, K. B. Eisenthal, T. F. Heinz, *Second-Harmonic Rayleigh Scattering from a Sphere of Centrosymmetric Material.* Physical Review Letters, 1999. **83**: p. 4045.
24. J. I. Dadap, J. Shan, T. F. Heinz, *Theory of optical second-harmonic generation from a sphere of centrosymmetric material: small-particle limit.* Journal of the Optical Society of America B, 2004. **21**(7): p. 1328-1347.
25. J. Nappa, I. Russier-Antoine, E. Benichou, C. Jonin, P-F. Brevet, *Wavelength dependence of the retardation effects in silver nanoparticles followed by polarization resolved hyper Rayleigh scattering.* Chemical Physics Letters, 2005. **415**: p. 246-250.
26. P. B. Johnson, R. W. Christy, *Optical Constants of the Noble Metals.* Physical Review B, 1972. **6**: p. 4370.

27. S. Brasselet, J. Zyss, *Multipolar molecules and multipolar fields: probing and controlling the tensorial nature of nonlinear molecular media.* Journal of the Optical Society of America B, 1998. **15**(1): p. 257-288.
28. I. Russier-Antoine, E. Benichou, G. Bachelier, C. Jonin, P-F. Brevet, *Multipolar Contributions of the Second Harmonic Generation from Silver and Gold Nanoparticles.* The Journal of Physical Chemistry C, 2007. **111**(26): p. 9044-9048.
29. J. Butet, G. Bachelier, I. Russier-Antoine, C. Jonin, E. Benichou, P.-F. Brevet, *Interference between Selected Dipoles and Octupoles in the Optical Second-Harmonic Generation from Spherical Gold Nanoparticles.* Physical Review Letters, 2010. **105**: p. 077401.
30. J. Nappa, I. Russier-Antoine, E. Benichou, C. Jonin, P-F. Brevet, *Second harmonic generation from small gold metallic particles: From the dipolar to the quadrupolar response.* The Journal of Chemical Physics, 2006. **125**.
31. J. Duboisset, P-F. Brevet, *Second-Harmonic Scattering-Defined Topological Classes for Nano-Objects.* The Journal of Physical Chemistry C, 2019. **123**(41): p. 25303-25308.
32. G-C. Li, D. Lei, M. Qiu, W. Jin, S. Lan, A. V. Zayats, *Light-induced symmetry breaking for enhancing second-harmonic generation from an ultrathin plasmonic nanocavity.* Nature Communications, 2021. **12**.